RSC Advances

PAPER

View Article Online
View Journal | View Issue

Cite this: *RSC Adv.*, 2023, **13**, 21545

The role of electrostatic potential in the translocation of triangulene across membranes†

Xiaofeng Tang, ‡*[a] Youyun Li,‡[b] Qianyan Li,[a] Jinhui Yu[a] and Han Bai*[ac]

Triangulene and its derivatives show broad application prospects in the fields of biological imaging and biosensing. However, its interaction with cell membranes is still poorly studied. In this study, classical molecular dynamics simulations were used to adjust the electrostatic potential of triangulene to observe its interactions with cell membranes. We found that electrostatic potential not only affects the behavior as it enters the cell membrane, but also spatial distribution within the cell membrane. The angle distribution of inside-0 and all-0 triangulene when penetrating the membrane is more extensive than that of ESP triangulene. However, inside-0 triangulene could cross the midline of the cell membrane and prefers to stay in the upper leaflet, while all-0 triangulene and ESP triangulene can reach the lower leaflet. These findings can help us regulate the distribution of nanoparticles in cells, so as to design functional nanoparticles that conform to the requirements.

Received 16th May 2023
Accepted 30th June 2023

DOI: 10.1039/d3ra03259k

rsc.li/rsc-advances

1. Introduction

Recent years have witnessed a spurt of progress in nanotechnology, and nanomaterials have shown increasing potential in biomedical fields such as targeted drug delivery, radiosensitization, and bioimaging.[1–4] The cell membrane is the first barrier for the interaction between biological systems against nanoparticles, and its interaction with nanoparticles will be the beginning of a series of subsequent reactions.[5–7] Hence, figuring out how nanoparticles interact with the cell membrane is crucial. It has been demonstrated that surface charge of nanoparticles has the potential to regulate the way they interact with cell membranes. For example, the periodically distributed electrostatic potential of C_2N nanosheets can prevent it from damaging the cell membrane.[8] Moreover, our recent research has found that the more polarized electrostatic potential of graphene quantum dots makes it harder to enter the cell membrane.[9] Besides, because of the highly polar nature of the head group of phospholipid molecules of cell membranes, it has been recognized that modulating the electrostatic potential (EP) of nanomaterials is one of the most effective methods to regulate the nanoparticle–cell membrane interactions.[10,11] Therefore, it is essential to understand how electrostatic potential (EP) of nanomaterials plays a role in the translocation across membranes. This can help us regulate the location of nanoparticles in the cell and design the required functional nanoparticles.

Triangulene is one of the most famous triplet-ground-state benzenoid hydrocarbons with interesting biological properties.[12–14] Yu created a benchmark dataset of 25 magnetic systems with nonlocal spin densities that can more accurately predict electronic ground state for triangulene analogues.[15] Shen introduced a new intramolecular radical–radical coupling approach and successfully synthesize two fused triangulene dimers efficiently.[16] Arikawa synthesized a kinetically-stabilized nitrogen-doped triangulene cation derivative.[17] Besides, atomic force microscopy (AFM) appears as an invaluable experimental technique, allowing the measurement of the mechanical strength of biomolecular complexes to provide a quantitative characterization of their interaction properties from a single molecule perspective.[18] The above research indicates that stable triangulene may be synthesized in the future, and tools such as AFM may help us analyze the interaction process between triangulene and cell membrane in experiments.[19] Recent research has found that the uniformly distributed electrostatic potential allows the system to have a small permanent dipole moment that blocks the electronic transition in the light excitation such that the electronic transition can only be carried out between adjacent carbon atoms.[14] According to the calculation of density functional theory (DFT), the derivatives of triangulene have high affinity for DNA helix.[20–23] Nevertheless, there are different mechanisms in healthy tissues and tumours. Unlike the non-toxic buckled form in healthy tissues, in tumours with relatively low pH values, the derivatives can intercalate DNA double

[a]*Yunnan Cancer Hospital, The Third Affiliated Hospital of Kunming Medical University, Kunming, People's Republic of China. E-mail: tangxiaofeng2023@163.com; bh001925@163.com*

[b]*The Second Affiliated Hospital of Kunming Medical University, Kunming, People's Republic of China*

[c]*School of Physics and Astronomy, Yunnan University, Kunming, People's Republic of China*

† Electronic supplementary information (ESI) available. See DOI: https://doi.org/10.1039/d3ra03259k

‡ Xiaofeng Tang and Youyun Li contributed equally to this work.

stranded base pairs in a planar form to disrupt biological processes, showing their potential anti-cancer properties.[13] In addition, the derivatives of triangulene can be used for specifically labeling cell mitochondria, lysosomes and other organelles with cell structures well preserved, thereby allow for various applications in the fields of biosensing and imaging due their excellent photo-physical properties.[24,25] However, the interaction mechanism between the electrostatic potential of triangulene and cell membrane is unrevealed, which limits its application in biomedicine.

In this study, we simulated the translocation of triangulene with different electrostatic potential in the cell membrane. Since 1-palmitoyl-2-oleoylphosphatidylcholine (POPC) is among the primary constituents of cellular membranes, it is often used to mimic eukaryote cell membrane.[26] Classical molecular dynamics (MD) simulations were employed to illustrate the binding dynamics of triangulene to the 1-palmitoyl-2-oleoylphosphatidylcholine (POPC) membrane. We constructed three groups of triangulene with different potentials, one of which had edges with potential polarity (inside-0), another group of evenly distributed potentials (ESP), and the third group with their potentials ignored (all-0).

2. Models and methods

2.1. System setup

As shown in Fig. 1, we constructed three groups of triangulene with different potentials. The net charge of each triangulene is 0e (shown in the S1†), and the force field parameters are derived from previous studies.[27,28] The first group of triangulene atomic charges are calculated by DFT which is called ESP.[29] The second group of triangulene atomic charges are acquired from ref. 16, the partial charges of hydrogen atoms and the linked carbon atoms were set to +0.115e and −0.115e, while carbon atoms away from the edge remained neutral.[28] The third group of triangulene atomic charges were assigned neutral charge. The electrostatic potential of triangulene are calculated by Adaptive Poisson–Boltzmann Solver (APBS).[30–32] The triangulene are placed on a plane parallel to the x–y plane, about 3 nm from the center of the POPC membrane. The side length of triangulene is 0.925 nm. In the MD simulation, 188 POPC lipids were used with 94 lipids in each layer. The POPC membrane was equilibrated at 100 ps in NPT ensemble. The solvent added to the system is the TIP3P-water molecules, and the size of the box is 7.64 nm × 7.64 nm × 10 nm.[33] The whole system was filled with 0.15 mol L^{-1} NaCl (44 Na^+ and Cl^-) to mimic the physiological environment (shown in the S2†).

2.2. Simulation parameters

All MD simulations were performed using the GROMACS package (version 4.6.7) with a time step of 2 fs. The parameters of the POPC lipid membrane were derived from the Charmm36 force field.[34] The minimized system by the steepest descent method accepted a 2 ns NPT ensemble pre-equilibration. The v-rescale thermostat and semiisotropic Parrinello–Rahman barostat matained the pressure of the system at 1 atm and the temperature at 310 K.[35,36] The short-range electrostatic and van der Waals interaction cut off distance was set to 1.2 nm, and the long-range electrostatic interaction was treated by the particle-mesh Ewald (PME) algorithm.[37] The SETTLE algorithm was used for the water model, and all heavy atoms connected to H atoms were constrained using the LINCS algorithm.[38,39] More details are available in our previous search.[9]

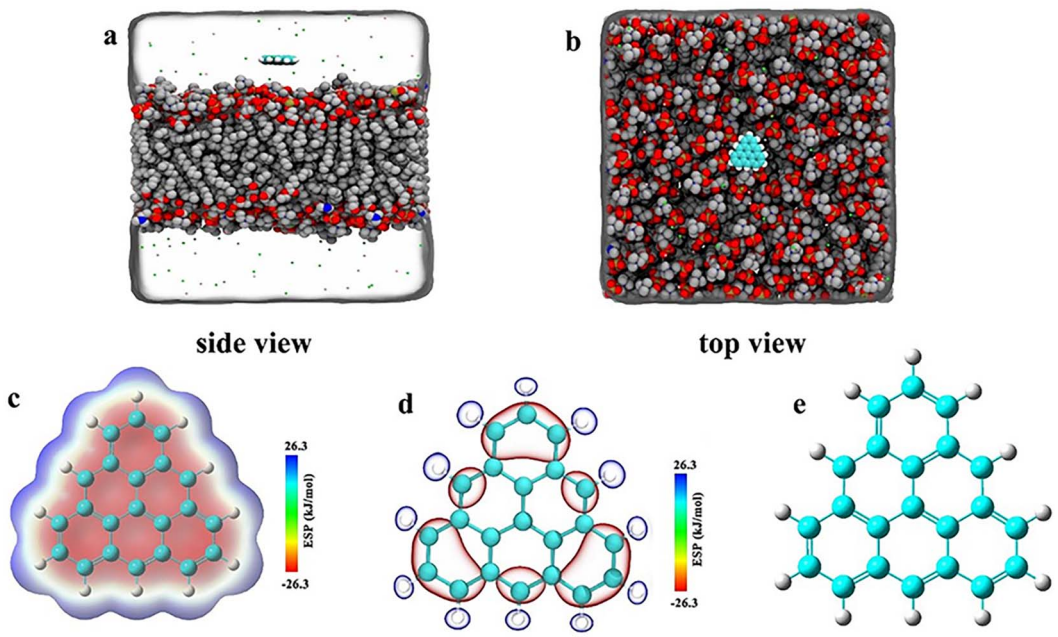

Fig. 1 The initial placement position of the system. (a) Side view (b) top view. (c), (d), and (e) Corresponding to surface distribution of electrostatic potential of ESP triangulene, inside-0 triangulene and all-0 triangulene, respectively.

2.3. Potential of mean force (PMF) calculation

By analyzing the three different electrostatic potential of the triangulene through the membrane process, we can calculate the free energy, thus explaining why the triangulene will finally stay. To compute the free energy profile along the Z axis we employ an umbrella sampling method.[40] Pulling triangulene from 0 nm (center of mass of POPC membrane) to 3.4 nm along the Z axis, with an umbrella sampling window of 0.1 nm. The constraining force constant was 2000 kJ mol^{-1} nm^{-2}. Notedly, the constraining force was only used for umbrella sampling to calculate PMF, while not imposed on the triangulation during MD simulation. The PMF curve is obtained by g_wham the tool.[41]

3. Results and discussion

3.1. Angular distribution of triangulene translocation across the POPC membrane

The whole system was divided into three regions along the Z axis, 5 nm to 2 nm was defined as region I (bulk water region), 2 nm to 0 nm was region II (upper leaflet), 0 to −2 nm was region III (lower leaflet). Relationship between angular distribution of triangulene and energy barrier was investigated. We found that ESP triangulene is easier to enter the membrane at an angle of 90° when permeating the membrane (Fig. 2b). However, inside-0 triangulene was more extensive when translocating into the membrane. It had the lowest energy barrier from 45 to 90° for inside-0 triangulene to mitigate from bulk water to upper leaflet (Fig. 2c). The all-0 triangulene was more effortless to enter the membrane at angles of 70, 90, 110 and 120° (Fig. 2d). As shown in Fig. 2, ESP triangulene and all-0 triangulene can get into the membrane and can ulteriorly cross the middle of the membrane to the lower leaflet, with the lowest energy barrier at 0.8 nm and −0.8 nm. While, the inside-0 triangulene can only get the upper leaflet of the membrane and preferred to remain in the upper layer region.

3.2. The spatial distribution of triangulene in the system

These three types of triangulene moved irregularly outside the membrane, whereas their behaviors changed obviously after entering the membrane (Fig. 3). The inside-0 triangulene had been slightly fluctuated and kept in region II (upper leaflet). ESP triangulene had been stayed mostly in region II, occasionally passing through the midline to the region III (lower leaflet). All-0 triangulene moved back and forth along the POPC membrane's center, and the time between the region II and region III was roughly equal. The results showed that the electrostatic potential of triangulene would have a significant effect on its spatial distribution in the POPC membrane.

3.3. The potential of mean force (PMF) of triangulene translocating into POPC

To further explain the reasons above spatial distribution occurs, the mean force potential (PMF) from 5 nm to −2 nm of triangulene was calculated (Fig. 4). The ΔW_1, ΔW_2 and ΔW_3 were

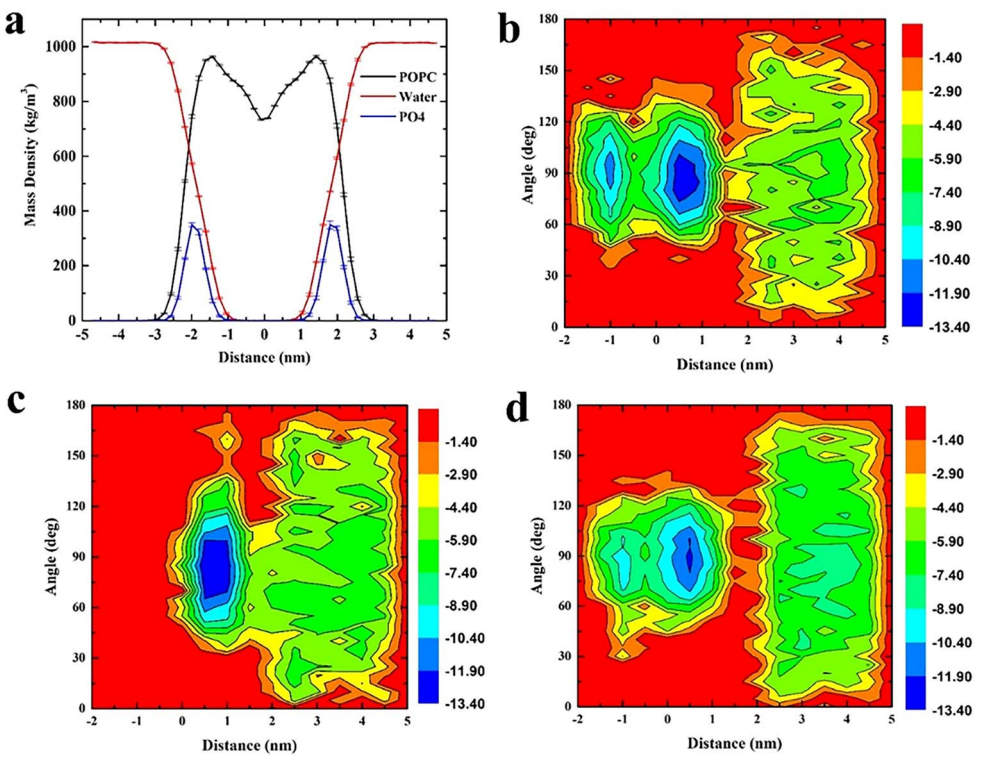

Fig. 2 (a) Density distribution of POPC membrane, water and phosphate group, defining the boundary of membrane at 2 nm. (b), (c), and (d) respectively show the distribution of angle (formed by ESP, inside-0 and all-0 triangulene surfaces and membrane surfaces) and the energy barrier along the Z axis during translocation.

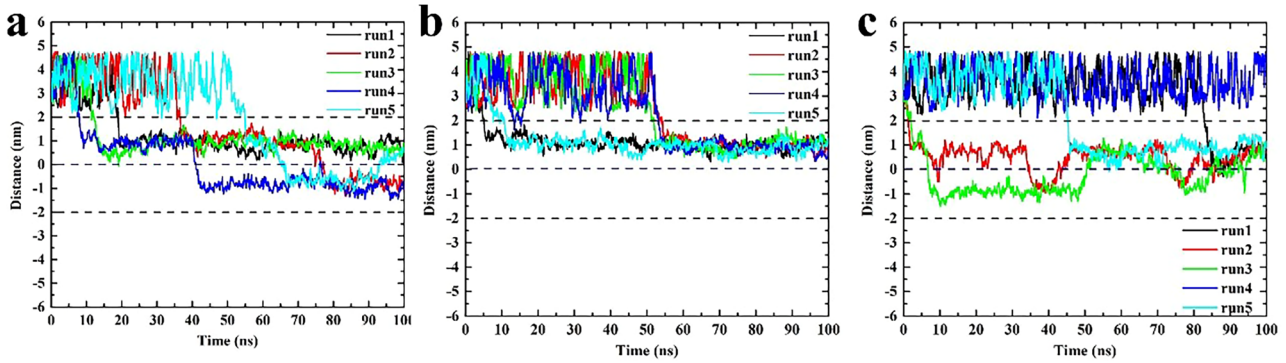

Fig. 3 The spatial distribution of triangulene in the POPC membrane. (a) ESP triangulene. (b) Inside-0 triangulene. (c) All-0 triangulene.

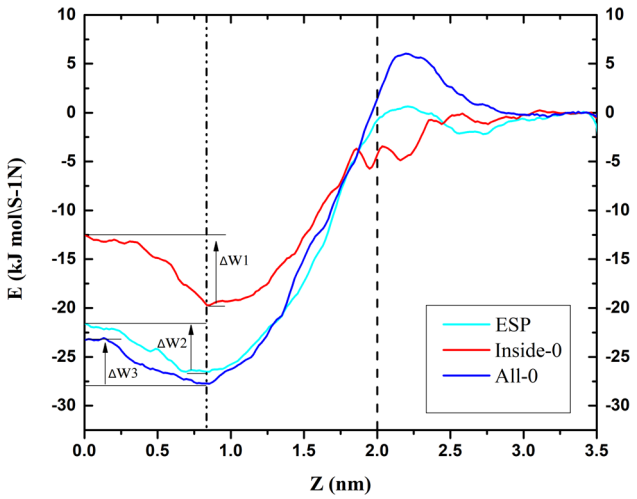

Fig. 4 The potential of mean force (PMF) of triangulene translocating into POPC along the *z*-axis direction.

defined as the PMF of ESP triangulene, inside-0 triangulene and all-0 triangulene in the midline of the membrane minus the lowest in the region II. The ESP triangulene and all-0 triangulene needed to overcome 4.84 kJ mol^{-1} (ΔW_1), 4.51 kJ mol^{-1} (ΔW_3) to reach the lower leaflet. Inside-0 triangulene needed to overcome 7.15 kJ mol^{-1} (ΔW_2), which explains why the inside-0 triangulene is only stayed in the upper leaflet of the membrane. However, ESP triangulene and all-0 triangulene can reach the lower leaflet of the membrane. From 5 nm to −2 nm, the energy at 0.8 nm is the lowest, so triangulene finally stay at 0.8 nm.

4. Conclusion

In this study, the effect of electrostatic potential on the interaction between triangulene and cell membrane were described by setting three kinds of triangulene models with different electrostatic potential distributions. We can conclude that: (1) the angle of ESP triangulene penetrated POPC membrane is mainly 90°, and can cross the midline of the membrane to the opposite side. The angle distribution of inside-0 triangulene penetrated is more extensive than that of ESP. The energy barrier is lower when penetrating the membrane from 45° to 90°, which makes it easier to penetrate the membrane, but it is difficult to cross the central line of the cell membrane. The angle distribution of all-0 triangulene penetrate membrane is more discrete, the energy barrier is lower at 70°, 90°, 110° and 120°, easy to penetrate into the membrane, and can also cross the cell membrane midline to reach the lower leaflet of the POPC membrane; (2) through PMF calculation, it is found that ESP, inside-0 and all-0 triangulene respectively need to overcome 4.84 kJ mol^{-1} (ΔW_1), 7.15 kJ mol^{-1} (ΔW_2) and 4.51 kJ mol^{-1} (ΔW_3). Therefore, inside-0 triangulene can hardly reach the lower leaflet due to the high energy barrier; (3) among these three systems, the energy barrier of the triangulene system is the lowest at 0.8 nm or −0.8 nm, that is the reason they finally stays at there.

Our research suggests the feasibility of regulating the interaction between triangulene and cell membrane through electrostatic potential, which would be helpful for further application of triangulene in biomedicine.

Abbreviations

MD	Classical molecular dynamics
POPC	1-Palmitoyl-2-oleoylphosphatidylcholine
DFT	Density functional theory
EP	Electrostatic potential
APBS	Adaptive Poisson–Boltzmann solver

Author contributions

The manuscript was written through contributions of all authors. All authors have given approval to the final version of the manuscript.

Conflicts of interest

The authors declare no competing financial interest.

Acknowledgements

We acknowledge financial support by Science, Technology Department of Yunnan Province (202101AY070001-164).

References

1 X. Chen and W. Zhang, *Chem. Soc. Rev.*, 2017, **46**, 734–760.
2 H. Wang, Q. Chen and S. Zhou, *Chem. Soc. Rev.*, 2018, **47**, 4198–4232.
3 H. Kang, J. Gravier, K. Bao, H. Wada, J. H. Lee, Y. Baek, G. El Fakhri, S. Gioux, B. P. Rubin, J. L. Coll and H. S. Choi, *Adv. Mater.*, 2016, **28**, 8162–8168.
4 H. M. Xiong, *Adv. Mater.*, 2013, **25**, 5329–5335.
5 X. Wang, X. Wang, X. Bai, L. Yan, T. Liu, M. Wang, Y. Song, G. Hu, Z. Gu, Q. Miao and C. Chen, *Nano Lett.*, 2019, **19**, 8–18.
6 F. Fontana, H. Lindstedt, A. Correia, J. Chiaro, O. K. Kari, J. Ndika, H. Alenius, J. Buck, S. Sieber, E. Makila, J. Salonen, A. Urtti, V. Cerullo, J. T. Hirvonen and H. A. Santos, *Adv. Healthcare Mater.*, 2020, **9**, 2000529.
7 D. Zou, Z. Wu, X. Yi, Y. Hui, G. Yang, Y. Liu, Tengjisi, H. Wang, A. Brooks, H. Wang, X. Liu, Z. P. Xu, M. S. Roberts, H. Gao and C. X. Zhao, *Proc. Natl. Acad. Sci. U. S. A.*, 2023, **120**, e2214757120.
8 S. Zhang, L. Liu, G. Duan, L. Zhao, S. Liu, B. Zhou and Z. Yang, *ACS Appl. Mater. Interfaces*, 2019, **11**, 34575–34585.
9 X. Tang, S. Zhang, H. Zhou, B. Zhou, S. Liu and Z. Yang, *Nanoscale*, 2020, **12**, 2732–2739.
10 P. Chen, Z. Huang, J. Liang, T. Cui, X. Zhang, B. Miao and L. T. Yan, *ACS Nano*, 2016, **10**, 11541–11547.
11 C. Pagnout, S. Jomini, M. Dadhwal, C. Caillet, F. Thomas and P. Bauda, *Colloids Surf., B*, 2012, **92**, 315–321.
12 S. Arikawa, A. Shimizu, D. Shiomi, K. Sato and R. Shintani, *J. Am. Chem. Soc.*, 2021, **143**, 19599–19605.
13 E. Leung, L. I. Pilkington, M. M. Naiya, D. Barker, A. Zafar, C. Eurtivong and J. Reynisson, *MedChemComm*, 2019, **10**, 1881–1891.
14 N. Zhang, W. Feng, H. Wen, N. Feng, H. Sheng, Z. Huang and J. Wang, *Molecules*, 2023, **28**, 3744.
15 H. Yu, J. Sun and T. Heine, *J. Chem. Theory Comput.*, 2023, **19**, 3486–3497.
16 T. Shen, D. Dijkstra, A. Farrando-Perez, P. G. Boj, J. M. Villalvilla, J. A. Quintana, Y. Zou, X. Hou, H. Wei, Z. Li, Z. Sun, M. A. Diaz-Garcia and J. Wu, *Angew. Chem., Int. Ed.*, 2023, **62**, e202304197.
17 S. Arikawa, A. Shimizu, D. Shiomi, K. Sato, T. Takui, H. Sotome, H. Miyasaka, M. Murai, S. Yamaguchi and R. Shintani, *Angew. Chem., Int. Ed.*, 2023, **62**, e202302714.
18 A. Lostao, K. Lim, M. C. Pallares, A. Ptak and C. Marcuello, *Int. J. Biol. Macromol.*, 2023, **238**, 124089.
19 E. Escorihuela, A. Concellón, I. Marín, V. J. Kumar, L. Herrer, S. A. Moggach, A. Vezzoli, R. J. Nichols, P. J. Low, P. Cea, J. L. Serrano and S. Martín, *Mater. Today Chem.*, 2022, **26**, 101067.
20 J. Reynisson, G. B. Schuster, S. B. Howerton, L. D. Williams, R. N. Barnett, C. L. Cleveland, U. Landman, N. Harrit and J. B. Chaires, *J. Am. Chem. Soc.*, 2003, **125**, 2072–2083.
21 A. Pothukuchy, S. Ellapan, K. R. Gopidas and M. Salazar, *Bioorg. Med. Chem. Lett.*, 2003, **13**, 1491–1494.
22 A. Kotar, B. Wang, A. Shivalingam, J. Gonzalez-Garcia, R. Vilar and J. Plavec, *Angew. Chem., Int. Ed.*, 2016, **55**, 12508–12511.
23 H. Yu, J. Sun and T. Heine, *J. Chem. Theory Comput.*, 2023, **19**, 3486–3497.
24 J. Bosson, J. Gouin and J. Lacour, *Chem. Soc. Rev.*, 2014, **43**, 2824–2840.
25 C. Bauer, R. Duwald, G. M. Labrador, S. Pascal, P. M. Lorente, J. Bosson, J. Lacour and J. D. Rochaix, *Org. Biomol. Chem.*, 2018, **16**, 919–923.
26 M. Mijajlovic, D. Wright, V. Zivkovic, J. X. Bi and M. J. Biggs, *Colloids Surf., B*, 2013, **104**, 276–281.
27 L. Liang, Z. Kong, Z. Kang, H. Wang, L. Zhang and J. W. Shen, *ACS Biomater. Sci. Eng.*, 2016, **2**, 1983–1991.
28 D. Cohen-Tanugi and J. C. Grossman, *Nano Lett.*, 2012, **12**, 3602–3608.
29 O. A. Gapurenko, A. G. Starikov, R. M. Minyaev and V. I. Minkin, *J. Comput. Chem.*, 2015, **36**, 2193–2199.
30 N. A. Baker, D. Sept, S. Joseph, M. J. Holst and J. A. McCammon, *Proc. Natl. Acad. Sci. U. S. A.*, 2001, **98**, 10037–10041.
31 T. J. Dolinsky, P. Czodrowski, H. Li, J. E. Nielsen, J. H. Jensen, G. Klebe and N. A. Baker, *Nucleic Acids Res.*, 2007, **35**, W522–W525.
32 A. S. Mamidi, A. Ray and N. Surolia, *Front. Bioeng. Biotechnol.*, 2019, **7**, 240.
33 W. L. Jorgensen, J. Chandrasekhar, J. D. Madura, R. W. Impey and M. L. Klein, *J. Chem. Phys.*, 1983, **79**, 926–935.
34 J. Huang and A. D. Mackerell, *J. Comput. Chem.*, 2013, **34**, 2135–2145.
35 G. Bussi, D. Donadio and M. Parrinello, *J. Chem. Phys.*, 2007, **126**, 014101.
36 M. Parrinello and A. Rahman, *J. Appl. Phys.*, 1998, **52**, 7182–7190.
37 T. Darden, D. York and L. Pedersen, *J. Chem. Phys.*, 1993, **98**, 10089–10092.
38 S. Miyamoto and P. A. Kollman, *J. Comput. Chem.*, 2010, **13**, 952–962.
39 B. Hess, H. Bekker and J. G. E. M. Fraaije, *J. Comput. Chem.*, 1997, **18**, 1463–1472.
40 G. M. Torrie and J. P. Valleau, *J. Chem. Phys.*, 1977, **66**, 1402–1408.
41 J. S. Hub, *J. Chem. Phys.*, 2015, **6**, 3713–3720.